

Anisotropic Hubbard model on a triangular lattice — spin dynamics in HoMnO₃

Saptarshi Ghosh* and Avinash Singh†

Department of Physics, Indian Institute of Technology Kanpur - 208016

The recent neutron-scattering data for spin-wave dispersion in HoMnO₃ are well described by an anisotropic Hubbard model on a triangular lattice with a planar (XY) spin anisotropy. Best fit indicates that magnetic excitations in HoMnO₃ correspond to the strong-coupling limit $U/t > \sim 15$, with planar exchange energy $J = 4t^2/U \simeq 2.5\text{meV}$ and planar anisotropy $\Delta U \simeq 0.35\text{meV}$.

There has been renewed interest in correlated electron systems on triangular lattices, as evidenced by recent studies of antiferromagnetism, superconductivity and metal-insulator transition in the organic systems $\kappa - (\text{BEDT} - \text{TTF})_2\text{X}$,^{1,2} the discovery of superconductivity in $\text{Na}_x\text{CoO}_2 \cdot y\text{H}_2\text{O}$,³ the observation of low-temperature insulating phases in some $\sqrt{3}$ -adlayer structures such as K on Si[111],⁴ and quasi two-dimensional 120° spin ordering and spin-wave excitations in $\text{RbFe}(\text{MoO}_4)_2$ (Refs. 5,6) and the multiferroic materials YMnO_3 and HoMnO_3 .^{7,8}

Recent neutron-scattering studies of the multiferroic material HoMnO_3 have revealed a non-collinear 120° antiferromagnetic (AF) ordering below $T_N \approx 72\text{ K}$ of the $S = 2\text{ Mn}^{3+}$ spins arranged in offset layers of two-dimensional (2D) triangular lattice.⁷ Measurements of the spin wave dispersion were found to be well described by a nearest-neighbour Heisenberg AF with exchange energy $J = 2.44\text{ meV}$ and a planar anisotropy $D = 0.38\text{ meV}$ at 20 K. No discernible dispersion was observed in the out-of-plane direction, indicating primarily 2D spin dynamics.

Recently spin-wave excitations in the 120° AF state of the Hubbard model on a triangular lattice were studied within the random phase approximation (RPA) in the full U range.⁹ The spin wave energy in the large U limit was shown to asymptotically approach the corresponding result for the Quantum Heisenberg antiferromagnet (QHAF), thus providing a continuous interpolation between weak and strong coupling limits. However, competing interactions and frustration were found to significantly modify the dispersion at finite U , resulting in vanishing spin stiffness at $U \approx 6$ and a magnetic instability at $U \approx 7$ corresponding to vanishing spin-wave energy at wave vector $\mathbf{q}_M = (\pi/3, \pi/\sqrt{3})$. The sharp fall-off of ω_M near $U \approx 7$ provides a sensitive indicator of finite- U effects in the AF state. Indeed, recent high-resolution neutron-scattering studies of the spin-wave dispersion in the square-lattice $S=1/2$ AF La_2CuO_4 have revealed noticeable spin-wave dispersion along the MBZ edge,¹⁰ associated with finite- U double-occupancy effects.¹¹

In this brief report we extend the spin-wave analysis to include planar spin anisotropy, and show that the neutron-scattering data for HoMnO_3 are also well described by a Hubbard model on a triangular lattice, thus providing a microscopic description of the most essential features of spin dynamics in the 120° AF state of HoMnO_3 , including the spin-wave dispersion and energy

scale. We examine the behaviour of spin-wave anisotropy gap with spin anisotropy and also suggest a sensitive measure of finite- U , double occupancy effects.

However, the Mn spin planar anisotropy is treated here only at a phenomenological level, equivalent to the effective anisotropy DS_{iz}^2 included in recent investigations using spin models.^{7,8} In a detailed study of single-ion anisotropy and crystal-field effects in the layered rare-earth cuprates R_2CuO_4 ($\text{R}=\text{Nd, Pr, Sm}$), the magnetic behaviour (including spin-reorientation transitions) has been attributed to coupling of Cu with the rare-earth magnetic subsystem which exhibits a large single-ion anisotropy resulting in preferential ordering of rare-earth moments along specific lattice directions.¹² It has been suggested that the anisotropy of Mn spins, its observed temperature dependence, and the reorientation transitions in HoMnO_3 also originate from a similar anisotropic exchange coupling with the rare-earth Holmium,⁷ resulting in magnetic behaviour as seen in layered rare-earth cuprates, where frustrated interlayer coupling allows for weaker, higher-order interactions to control the magnetic structure. Especially relevant for non-collinear ordering, the anisotropic exchange (Dzyaloshinski-Moriya) interaction $\mathbf{D} \cdot (\mathbf{S}_i \times \mathbf{S}_j)$ originating from spin-orbit coupling has been suggested as responsible for the clamping of ferroelectric and antiferromagnetic order parameters in YMnO_3 .¹³

Hund's rule coupling responsible for the $S = 2$ spin state of Mn^{+++} ions and crystal-field splitting have also not been realistically incorporated here. However, these realistic details do not qualitatively affect the spin-rotation symmetry and spin dynamics, as discussed below. Hund's rule coupling in the generalized Hubbard model considered here is maximal as inter-orbital Coulomb interaction for parallel spins is dropped completely. Including an inter-orbital density-density interaction V_0 and an intra-atomic exchange interaction F_0 favouring parallel-spin alignment (Hund's rule coupling), the more realistic orbital Hubbard model^{14,15}

$$\begin{aligned}
 H = & -t \sum_{i,\delta,\gamma,\sigma} a_{i\gamma\sigma}^\dagger a_{i+\delta,\gamma\sigma} + U \sum_{i\gamma} n_{i\gamma\uparrow} n_{i\gamma\downarrow} \\
 & + \sum_{i,\gamma < \gamma',\sigma,\sigma'} (V_0 - \delta_{\sigma\sigma'} F_0) n_{i\gamma\sigma} n_{i\gamma'\sigma'} \\
 & + F_0 \sum_{i,\gamma < \gamma',\sigma \neq \sigma'} a_{i\gamma\sigma}^\dagger a_{i\gamma'\sigma} a_{i\gamma'\sigma'}^\dagger a_{i\gamma\sigma'} \quad (1)
 \end{aligned}$$

remains spin-rotationally invariant under a global rota-

tion of the fermion spin $\mathbf{S}_{i\gamma} = \Psi_{i\gamma}^\dagger \frac{\boldsymbol{\sigma}}{2} \Psi_{i\gamma}$ (where $\Psi_{i\gamma}^\dagger \equiv (a_{i\gamma\uparrow}^\dagger a_{i\gamma\downarrow}^\dagger)$ is the fermion field operator), even if orbitals γ are identified with the Mn orbitals (t_{2g}, e_g) resulting from crystal-field splitting of the atomic 3d orbitals. As the intra-atomic exchange interaction F_0 is much larger than the spin excitation energy scale ($\sim \frac{t^2}{U+F_0}$, within a strong-coupling expansion), all fermion spins on a site are effectively coupled, yielding a composite quantum spin S and a corresponding multiplication by factor $2S$ to obtain the effective spin-wave energy scale. Therefore, orbital multiplicity does not change the Goldstone-mode structure, and the spin-dynamics energy scale in the orbital Hubbard model is essentially determined by t and $U_{\text{eff}} = U + F_0$.

As a simplest extension to phenomenologically include spin-space anisotropy, while retaining only the relevant energy scales t and U_{eff} , we consider the generalized \mathcal{N} -orbital Hubbard model¹⁶

$$H = -t \sum_{i,\delta,\gamma,\sigma} a_{i\gamma\sigma}^\dagger a_{i+\delta,\gamma,\sigma} + \frac{U_1}{\mathcal{N}} \sum_{i,\gamma,\gamma'} a_{i\gamma\uparrow}^\dagger a_{i\gamma\uparrow} a_{i\gamma'\downarrow}^\dagger a_{i\gamma'\downarrow} + \frac{U_2}{\mathcal{N}} \sum_{i,\gamma,\gamma'} a_{i\gamma\uparrow}^\dagger a_{i\gamma'\uparrow} a_{i\gamma'\downarrow}^\dagger a_{i\gamma\downarrow} \quad (2)$$

on a triangular lattice with nearest-neighbour (NN) hopping between sites i and $i+\delta$. Here γ, γ' refer to the (fictitious) degenerate \mathcal{N} orbitals per site. The factor $\frac{1}{\mathcal{N}}$ is included to render the energy density finite in the $\mathcal{N} \rightarrow \infty$ limit. The two correlation terms involve density-density and exchange interactions with respect to the orbital indices. The Hartree-Fock (HF) approximation and Random Phase Approximation (RPA) are of $\mathcal{O}(1)$ whereas quantum fluctuation effects appear at higher order within the inverse-degeneracy expansion and thus $1/\mathcal{N}$, in analogy with $1/S$ for quantum spin systems, plays the role of \hbar .

The key feature of spin-rotation symmetry of the generalized Hubbard model is highlighted by writing the two interaction terms as

$$H_{\text{int}} = -\frac{U_2}{\mathcal{N}} \sum_i \mathbf{S}_i \cdot \mathbf{S}_i + \frac{U_2 - U_1}{\mathcal{N}} \sum_i S_{iz}^2 \quad (3)$$

in terms of the total spin operator

$$\mathbf{S}_i = \sum_\gamma \psi_{i\gamma}^\dagger \frac{\boldsymbol{\sigma}}{2} \psi_{i\gamma} \equiv \sum_\gamma \frac{\boldsymbol{\sigma}_{i\gamma}}{2} \quad (4)$$

where $\psi_{i\gamma}^\dagger \equiv (a_{i\gamma\uparrow}^\dagger a_{i\gamma\downarrow}^\dagger)$. An Ising (uniaxial) anisotropy is obtained for $U_1 > U_2$, a planar (XY) anisotropy for $U_2 > U_1$, and full spin-rotation symmetry for $U_1 = U_2$.

As appropriate for HoMnO₃, we consider the case $U_2 > U_1$ corresponding to preferential ordering of spins in the $x-y$ plane in spin space and an anisotropy gap for out-of-plane excitations.⁷ Magnetic excitations were analyzed in terms of a Heisenberg model with a similar anisotropy term in Ref. [7]. At the HF level, the interaction term

for orbital γ then reduces to

$$H_{\text{int}}^\gamma = - \sum_i \boldsymbol{\sigma}_{i\gamma} \cdot \boldsymbol{\Delta}_i \quad (5)$$

where the self-consistently determined mean field $\boldsymbol{\Delta}_i = U_2 \langle \mathbf{S}_{i\gamma'} \rangle_{\text{HF}}$ lies in the $x-y$ plane in spin space. The HF sublattice magnetization depends only on U_2 and is determined from the self-consistency condition $\langle \mathbf{S}_\alpha \rangle_{\text{HF}} = \sum_{\mathbf{k},l} \langle \mathbf{k}, l | \frac{\boldsymbol{\sigma}}{2} | \mathbf{k}, l \rangle_\alpha$ in terms of the HF states $|\mathbf{k}, l\rangle$ on sublattice α , exactly as for the isotropic case.⁹ In the strong coupling limit the sublattice magnetization $\langle \mathbf{S}_\alpha \rangle \approx 1/2$ at the HF level, and is reduced by about 50% (in the isotropic case) due to quantum fluctuations, as found in different calculations cited in Ref. [9].

We consider the 120° ordered AF state on the triangular lattice, and examine transverse spin fluctuations about the broken-symmetry state. At the RPA level, the magnon propagator reduces to a sum of all bubble diagrams where the interaction vertices involving S_{ix}^2 and S_{iy}^2 appear with interaction U_2 , whereas those involving S_{iz}^2 with interaction U_1 . Introducing a planar spin rotation, so that spins are oriented along the x' direction for all three sublattices, we obtain for the transverse spin-fluctuation propagator

$$[\chi(\mathbf{q}, \omega)]_{\alpha\beta}^{\mu\nu} = \frac{[\chi^0(\mathbf{q}, \omega)]}{1 - 2[U][\chi^0(\mathbf{q}, \omega)]} \quad (6)$$

in the $2 \otimes 3$ spin-sublattice basis of the two transverse spin directions $\mu, \nu = y', z'$ and the three sublattices $\alpha, \beta = A, B, C$. The sublattice-diagonal interaction matrix

$$[U] = \begin{bmatrix} U_2 \mathbf{1} & \mathbf{0} \\ \mathbf{0} & U_1 \mathbf{1} \end{bmatrix} \quad (7)$$

in the y', z' basis, and the bare particle-hole propagator

$$[\chi^0(\mathbf{q}, \omega)]_{\alpha\beta}^{\mu\nu} = \frac{1}{4} \sum_{\mathbf{k}, l, m} \left[\frac{\langle \sigma_\mu \rangle_\alpha^{--} \langle \sigma_\nu \rangle_\beta^{++}}{E_{\mathbf{k}-\mathbf{q}, m}^+ - E_{\mathbf{k}, l}^- + \omega} + \frac{\langle \sigma_\mu \rangle_\alpha^{+-} \langle \sigma_\nu \rangle_\beta^{*-}}{E_{\mathbf{k}, m}^+ - E_{\mathbf{k}-\mathbf{q}, l}^- - \omega} \right] \quad (8)$$

involves integrating out the fermions in the broken-symmetry state. In the particle-hole matrix elements

$$\langle \sigma_\mu \rangle_\alpha^{--} \equiv \langle \mathbf{k} - \mathbf{q}, m | \sigma_\mu | \mathbf{k}, l \rangle_\alpha \quad (9)$$

of the rotated spins, the spin orientation angles ϕ_α in the fermion states $|\mathbf{k}, l\rangle$ are transformed out. The numerical evaluation of $[\chi^0(\mathbf{q}, \omega)]$ in terms of the HF-level AF-state energies and amplitudes is exactly as for the isotropic case studied earlier.⁹

The spin-wave energies $\omega_{\mathbf{q}}$ are then obtained from the poles $1 - \lambda_{\mathbf{q}}(\omega_{\mathbf{q}}) = 0$ of Eq. (6) in terms of the eigenvalues $\lambda_{\mathbf{q}}(\omega)$ of the matrix $2[U][\chi^0(\mathbf{q}, \omega)]$. As $\omega_{\mathbf{q}}$ corresponds to spin 1/2, it is scaled by the factor $2S$ for arbitrary spin S .¹⁷ As expected for planar anisotropy, there is only

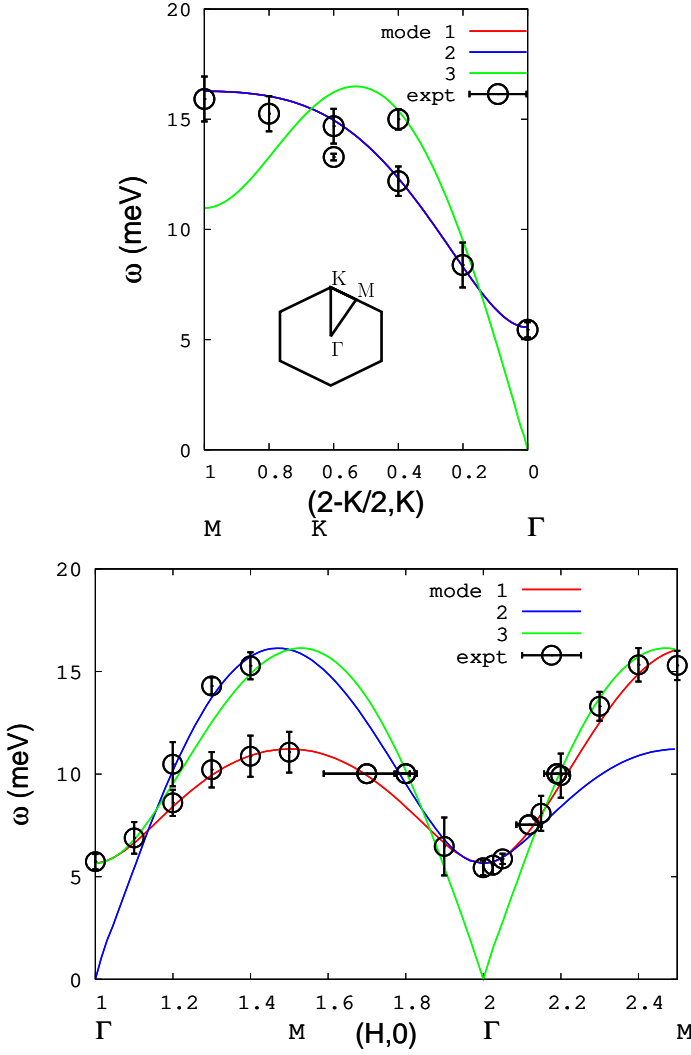


FIG. 1: (color online) Spin-wave dispersion for the three modes calculated from Eq. (5) with $J = 4t^2/U \approx 2.5\text{meV}$ and $\Delta U \approx 0.35\text{meV}$, along with neutron scattering data points for HoMnO_3 at 20K from Ref. [7].

one Goldstone mode corresponding to planar rotation of spins, and the two out-of-plane modes become massive with an anisotropy gap ω_{gap} .

Spin-wave dispersion $\omega_{\mathbf{q}}$ for the three modes is shown in Fig. 1 along two symmetry directions in the magnetic Brillouin zone (MBZ), along with the neutron-scattering data for HoMnO_3 at 20 K from Ref. [7]. The anisotropic Hubbard model provides a remarkably good description of the spin dynamics. We find that best fits with the magnetic excitations in HoMnO_3 are only obtained in the strong-coupling limit $U/t > \sim 15$, with a planar exchange energy $J = 4t^2/U \simeq 2.5\text{meV}$ and anisotropy $U_2 - U_1 \equiv \Delta U \simeq 0.35\text{meV}$, the individual values of t and U not being resolvable within experimental resolution. To estimate the order of magnitude of the ratio U/t , if we nominally take $U = 1\text{eV}$, we obtain $t = 25\text{meV}$ and

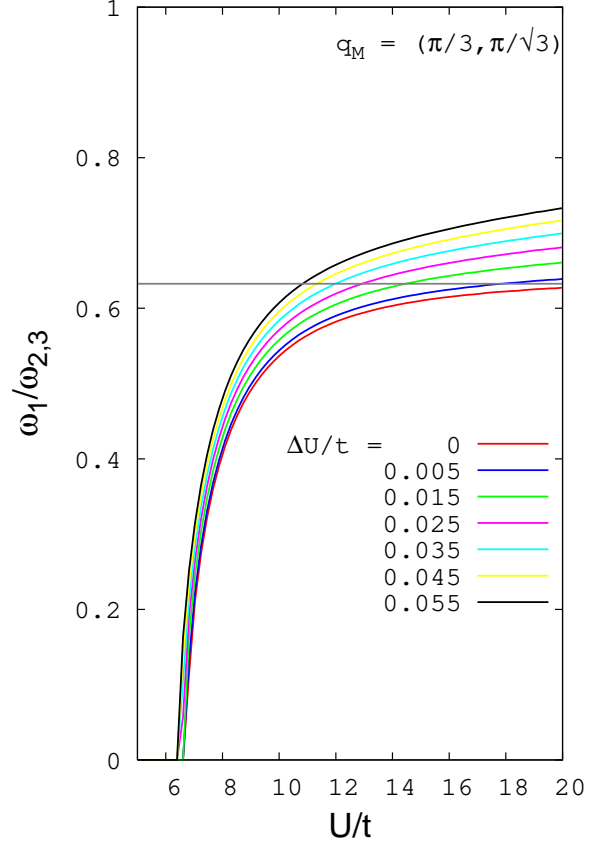


FIG. 2: (color online) The ratio $\omega_1/\omega_{2,3}$ at wave vector \mathbf{q}_M provides a sensitive indicator of finite- U , double-occupancy effects, shown for different values of spin anisotropy ΔU .

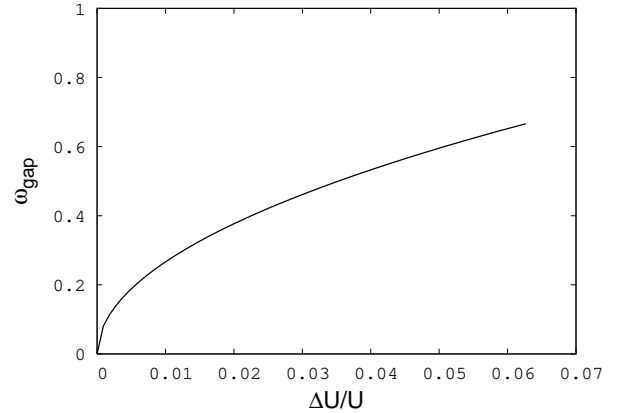


FIG. 3: Spin-wave anisotropy gap corresponding to out-of-plane fluctuations shows a $\sim (\Delta U/U)^{1/2}$ behaviour with spin anisotropy. Here $U/t = 16$.

$U/t = 40$. Spin-wave dispersion calculated in the intermediate coupling regime cannot be fitted with the neutron scattering data, indicating no evidence of finite- U double occupancy effects, as discussed below.

For the square-lattice $S = 1/2$ AF La_2CuO_4 , finite- U , double-occupancy effects associated with higher-order

(t^4/U^3) spin couplings are manifested in noticeable spin-wave dispersion along the MBZ boundary.^{10,11} Similarly, for the isotropic triangular-lattice AF, the ratio $\omega_1/\omega_{2,3}$ of the non-degenerate and degenerate spin-wave energies at wave vector $\mathbf{q}_M = (\pi/3, \pi/\sqrt{3})$ is a sensitive measure of the U/t ratio,⁹ which asymptotically approaches $2/\sqrt{10} = 0.632$ in the strong-coupling ($U/t \rightarrow \infty$) limit, decreases monotonically with U/t , and eventually vanishes at $U/t \approx 7$.⁹ Variation of $\omega_1/\omega_{2,3}$ with U/t is shown in Fig. 2 for different values of anisotropy $\Delta U/t$. Neutron-scattering data for HoMnO₃ shows that $\omega_1/\omega_{2,3} \approx 11\text{meV}/16\text{meV} \approx 0.7$, which yields a lower bound (~ 15) on the ratio U/t from Fig. 2.

The spin-wave anisotropy gap ω_{gap}/t , corresponding to out-of-plane fluctuations with $q = 0$, varies as $(\Delta U/U)^{1/2}$ with spin anisotropy (Fig. 3), which translates to $\omega_{\text{gap}} \propto \sqrt{J\Delta U}$, the geometric mean of the two energy scales.

In conclusion, the anisotropic Hubbard model provides a simple extension to phenomenologically include spin-space anisotropy and study spin excitations in the full range from weak to strong coupling. Comparison of spin-

wave dispersion with RPA calculations allows for a quantitative determination of the effective anisotropy, in addition to highlighting any finite- U , double occupancy effects as seen in La₂CuO₄. The recent neutron-scattering data for spin-wave dispersion in HoMnO₃ are found to be well described by an anisotropic Hubbard model on a triangular lattice with a planar (XY) spin anisotropy. We find that the twin constraints $\omega_{\text{gap}}/\omega_{1,2} \approx 1/3$ and $\omega_1/\omega_{2,3} \approx 2/3$ in the neutron scattering data cannot be satisfied in the intermediate coupling regime, and best fit indicates that magnetic excitations in HoMnO₃ correspond to the strong-coupling limit $U/t > \sim 15$, with $J \simeq 2.5\text{meV}$ and $\Delta U \simeq 0.35\text{meV}$. The ratio $\omega_1/\omega_{2,3}$ of the non-degenerate and degenerate spin-wave energies at wave vector $\mathbf{q}_M = (\pi/3, \pi/\sqrt{3})$ is suggested as a sensitive measure of finite- U , double occupancy effects in a triangular-lattice antiferromagnet. Finally, in view of the formal resemblance with the orbital Hubbard model (1), our RPA calculation provides a step forward towards investigating magnetic excitations using realistic models including Hund's rule coupling, crystal-field splitting etc.

* Electronic address: gsap@iitk.ac.in

† Electronic address: avinas@iitk.ac.in

¹ K. Kanoda, Physica C **282-287**, 299 (1997); K. Kanoda, Hyperfine Interact. **104**, 235 (1997).

² R. H. McKenzie, Science, **278**, 820 (1997).

³ K. Takada *et al.*, Nature **422**, 53 (2003).

⁴ H. H. Weitering, X. Shi, P. D. Johnson, J. Chen, N. J. Dinardo, and S. Kempa, Phys. Rev. Lett. **78**, 1331 (1997).

⁵ T. Inami, Y. Ajiro, and T. Goto, J. Phys. Soc. Jpn. **65**, 2374 (1996).

⁶ L. E. Svistov, A. I. Smirnov, L. A. Prozorova, O. A. Petrenko, L. N. Demianets, and A. Ya. Shapiro, Phys. Rev. B **67** 094 434 (2003).

⁷ O. P. Vajk, M. Kenzelmann, J. W. Lynn, S. B. Kim, and S.-W. Cheong, Phys. Rev. Lett. **94**, 087601 (2005).

⁸ T. J. Sato, S. -H. Lee, T. Katsufuji, M. Masaki, S. Park,

J. R. D. Copley, and H. Takagi, Phys. Rev. B **68**, 014432 (2003).

⁹ A. Singh, Phys. Rev. B **71**, 214406 (2005).

¹⁰ R. Coldea, S. M. Hayden, G. Aeppli, T. G. Perring, C. D. Frost, T. E. Mason, S.-W. Cheong, and Z. Fisk, Phys. Rev. Lett. **86**, 5377 (2001).

¹¹ A. Singh and P. Goswami, Phys. Rev. B **66**, 92402 (2002).

¹² R. Sachidanandam, T. Yildirim, A. B. Harris, A. Aharony, and O. E.-Wohlman, Phys. Rev. B **56**, 260 (1997).

¹³ E. Hanamura, K. Hagita, and Y. Tanabe, J. Phys.: Condens. Matter **15**, L103 (2003).

¹⁴ L. M. Roth, Phys. Rev. **149**, 306 (1966).

¹⁵ K. Held and D. Vollhardt, Eur. Phys. J. B **5**, 473 (1998).

¹⁶ A. Singh, Phys. Rev. B **43**, 3617 (1991).

¹⁷ A. Singh and P. Sen, Phys. Rev. B **57**, 10598 (1998).